MJFAS
Malaysian Journal of Fundamental and Applied Sciences

Ma *et al.* | Malaysian Journal of Fundamental and Applied Sciences, Vol. 20 (2024) 1172-1182

RESEARCH ARTICLE

Predictive Value of Multi-Phase CT Radiomics in Delineating Early and Advanced T Staging of Colon Cancer

Kun Ma[a], Haobo Shi[e], Tian Swee Tan[a,b*], Muhammad Amir As'ari[a,c], Yan Chai Hum[d], Jahanzeb Sheikh[a,f], Wei Huang[e], Kah Meng Leong[a,h], Matthias Foh Thye Tiong[a], Madeeha Sadia[g], Zhibo Wen[e]

[a]Department of Biomedical Engineering & Health Sciences, Faculty of Electrical Engineering, Universiti Teknologi Malaysia, 81310 UTM Johor Bahru, Johor, Malaysia; [b]IJN-UTM Cardiovascular Engineering Centre, Institute of Human Centered Engineering, Universiti Teknologi Malaysia, 81310 UTM Johor Bahru, Johor, Malaysia; [c]Sport Innovation & Technology Centre, Institute of Human Centered Engineering, Universiti Teknologi Malaysia, 81310 UTM Johor Bahru, Johor, Malaysia; [d]Department of Mechatronics and Biomedical Engineering, Lee Kong Chian Faculty of Engineering and Science, Universiti Tunku Abdul Rahman, Malaysia; [e]Department of Radiology, Zhujiang Hospital, Southern Medical University, Haizhu District, Guangzhou, Guangdong, China; [f]Department of Biomedical Engineering, Sir Syed University of Engineering &Technology, Karachi, Pakistan; [g]Department of Biomedical Engineering, NED University of Engineering and Technology, Pakistan; [h]Department of Electrical & Electronics Engineering, Faculty Of Engineering & Information Technology, Southern University College, Malaysia

Abstract This study leveraged the power of multi-phase CT radiomics, which extracts detailed features from multi-phase images, to explore the distinction between early (T1-T2) and advanced (T3-T4) colon cancer stages in each of multiple phases, providing valuable insights to healthcare professionals and enhancing their decision-making capabilities. A total of 191 patients with surgically confirmed primary colon cancer were retrospectively included, and multi-phase CT scans (non-enhanced contrast phase, arterial phase, portal venous phase, and delayed phase) were conducted within one week before surgery. Three-dimensional segmentation of colonic tumors was performed on the images of the four phases, and radiomics features of each colonic tumor were automatically extracted. Minimum redundancy maximum relevance (mRMR) was applied to features selection in each of the four phases. The least absolute shrinkage and selection operator logistic regression was conducted to determine the association between radiomics features and early (T1-T2) and advanced (T3-T4) stages of colon cancer. Additionally, diagnostic performance comparison was carried out in four phases. The mean (±SD) age of the 191 individuals was 61.87±13.137 years, with females comprising 43.5% of the cohort. The selected features for the non-enhanced, arterial, portal venous, and delayed phases numbered 7, 11, 6, and 10, respectively. In the test set, the AUC values for the on-enhanced, arterial, portal venous, and delayed phases were 0.86 (0.76-0.96), 0.84 (0.73-0.94), 0.82 (0.71-0.93), and 0.86 (0.75-0.97), with corresponding accuracies of 0.84, 0.80, 0.75, and 0.88, sensitivities of 0.73, 0.64, 0.86, and 0.68, and specificities of 0.91, 0.91, 0.68, and 1.00, respectively. DeLong's test revealed no statistically significant differences in the AUC values between the four phases within the test sets (P = 0.3233~ 0.9912). Multi-phase CT radiomics demonstrated substantial value in differentiating between early (T1-T2) and advanced (T3-T4) stages of patients with colon cancer.

Keywords: T staging, colon cancer, multiple-phase CT, radiomics.

***For correspondence:**
tantswee@utm.my

Received: 28 June 2024
Accepted: 11 Sept. 2024

Introduction

Colorectal cancer stands as the predominant malignant tumor affecting the digestive system globally, ranking third in incidence and second in mortality rates (1). Colon cancer comprises approximately 60%-70% of all colorectal cancer cases. In China, colon cancer accounts for about 50% of colorectal cancer cases (2). A discernible shift toward the affliction of a younger demographic by colon cancer has significantly impacted public health, exerting substantial economic burdens. Consequently, the imperative of both treating and preventing colon cancer cannot be overstated. Despite significant advancements in treatment, the early symptoms of the disease often evade detection, leading to delayed diagnoses that profoundly affect patient prognoses. Early detection of colon cancer and precise clinical staging are closely linked to the prognosis of the disease. Hence, meticulous preoperative clinical analysis plays an indispensable role in determining the most suitable treatment modalities for colon cancer (3). Tumors infiltrating different layers of the intestinal wall exhibit varied responses to surgical interventions at different stages. For tumors confined to the submucosa or muscularis propria without penetrating beyond the latter (T1-T2 stages), surgical excision is commonly employed. Conversely, for cases of colon cancer that have progressed beyond the muscularis propria (T3-T4 stages), personalized chemotherapy is recommended based on individual patient conditions to curtail recurrence rates and augment patient survival. Therefore, precise preoperative T staging is pivotal in dictating the appropriate treatment strategy for colon cancer.

Various methodologies, such as fibro-colonoscopy, MRI, and CT examinations, are commonly employed for preoperative T staging of colon cancer. However, colonoscopy with biopsy, a conventional method, presents inherent complexities and associated risks (4), while providing limited insights into the comprehensive physiological status of the tumor (5). MRI, characterized by high-resolution multi-angle imaging, particularly excels in delineating tumor infiltration within the intestines. However, certain patients may not be suitable candidates for MRI due to specific contraindications. In contrast, CT imaging enjoys widespread recognition for its rapid imaging capabilities, capacity to surmount artifacts, and comprehensive assessment of overall bodily conditions and distant metastases. The Union for International Cancer Control (UICC) endorses CT imaging as a routine screening modality for colon cancer among high-risk populations, for preoperative evaluations, and as part of follow-up protocols during adjuvant chemotherapy (6, 7).

However, the information gleaned from conventional CT scans is often constrained, relying on empirical approaches for analysis and diagnosis. In contrast to traditional imaging assessment methods, radiomics represents an emerging non-invasive multidisciplinary technology rooted in conventional imaging data. It involves extracting high-throughput quantitative features and transforming medical images into high-dimensional and exploitable data. In their study, Hong *et al.* (8) proposed the integration of radiomic features with CT imaging to predict T-staging in colon cancer patients, achieving a predictive performance of 0.727 for T3-T4 stages. This integration significantly enhanced the detection rate among high-risk colon cancer patients. Similarly, Caruso *et al*. (9) established a radiomic model for identifying high-risk colon cancer (T4) in non-metastatic colon cancer patients. Their model effectively stratified high-risk colon cancer cases, yielding an area under the curve (AUC) of 0.75 in an external cohort study. Additionally, researchers such as Ma *et al*. (10) employed radiomic features extracted from T2-weighted MRI images to predict rectal cancer T-staging (T1-T2 and T3-T3), achieving an accuracy of 0.762 in their predictive models.

However, the studies on CT-based T-staging prediction predominantly relied on single-phase imaging, specifically the portal venous phase (8, 9), for radiomic investigations of colon or rectal cancer. Despite their contribution, these studies exhibited relatively modest accuracy levels. There remains a scarcity of research exploring the potential of multi-phase CT (including non-enhanced, arterial, portal venous, and delayed phases) radiomics in distinguishing between T1-T2 and T3-T4 staging in colon cancer patients. Moreover, given the anatomical differences between colon and rectal cancer—particularly the fact that colon cancer has a serosal layer while rectal cancer does not—multi-phase CT radiomics could potentially offer more precise preoperative guidance for individuals with colon cancer.

Recognizing this research gap, we developed the least absolute shrinkage and selection operator (LASSO) regression model utilizing multi-phase CT scans of colon cancer patients. Our study aimed to compare staging performance across distinct phases and to evaluate the model's efficacy in staging. Our study endeavored to provide valuable insights to healthcare professionals, enhancing their ability to make well-informed decisions based on the staging performance of the model derived from various phases of CT imaging.

Materials and Methods

Patient Information

This retrospective study received approval from the institution's Ethics Review Committee (Zhujiang Hospital of Southern Medical University, ethics number: 2023-KY-226-01) and obtained an exemption from the requirement for patient informed consent. The cohort comprised 191 postoperative patients diagnosed with colon cancer at Zhujiang Hospital of Southern Medical University between January 2020 and August 2023, all pathologically confirmed.

The inclusion criteria encompassed: (1) cases pathologically confirmed as colon cancer post-surgery, (2) absence of contraindications for Multiple-slice CT (MSCT) examination (e.g., iodine allergy, hepatic or renal function impairment, congestive heart failure), (3) complete MSCT examination conducted within one week preceding surgery, covering non-enhanced, arterial, portal venous, and delayed phases, (4) absence of prior specific cancer treatments like radiotherapy or chemotherapy before surgery, and (5) availability of retrievable clinical data from the medical records system, including pathological details, gender, and age, with patients aged 18 years or older. Exclusion criteria comprised: (1) cases pathologically confirmed as rectal cancer post-surgery, (2) incomplete imaging from the four-phase MSCT examination before surgery, (3) concurrent malignancies in patients, and (4) insufficient clinical data or patient refusal to participate in the study.

CT Protocols

All patients underwent comprehensive preoperative MSCT examinations encompassing four-phase scans, including non-enhanced, arterial, portal venous, and delayed phase. Imaging data were meticulously collected utilizing state-of-the-art scanning devices, namely the Philips Brilliance series (64, 128) and Philips Brilliance iCT (256). Standardized scan parameters were employed, maintaining a tube voltage of 120 kV, utilizing automatic tube current modulation technology (DoseRight). The pitch was set at 0.925. For non-enhanced, arterial phase, and delayed phase reconstructions, the slice thickness and interval were set at 5 mm. For the portal venous phase, a slice thickness and interval were set at 1 mm. The scanning range spanned from the diaphragmatic dome to the lower margin of the pubic symphysis. Patients were positioned in a supine posture during the scan procedure, which commenced with a non-enhanced scan. Subsequently, a non-ionic contrast agent (iopromide, 370 mg I/mL) was administered through the median cubital vein using a power injector at a flow rate of 2.5 ml/second. Sequential scans were then performed at intervals of 30 seconds, 60 seconds, and 90 seconds post-injection to capture the arterial, portal venous, and delayed phases, respectively.

CT Image Analysis

Segmentation of all instances of colon cancer was conducted with utmost precision by an expert abdominal radiologist (Zhujiang Hospital of Southern Medical University, China). These proficient professionals executed meticulous volumetric segmentations of colon cancer from the preoperative CT scans, capturing the non-enhanced phase, arterial phase, portal venous phase, and delayed phase. The segmentation process utilized the open-source MITK software (version 2023.04, available at https://www.mitk.org/wiki/). To ensure an objective and unbiased analysis, the readers were kept blinded to all clinical and histological data, although essential information regarding the tumor's location was provided solely to facilitate accurate segmentation and qualitative assessment. The volumetric region of interest (ROI) underwent a thorough manual delineation, slice-by-slice, meticulously encompassing the entire volume occupied by colon cancer. Simultaneously, deliberate exclusion of the surrounding pericolic fat and healthy large bowel wall was executed from the segmentation process (see Figure 1). Finally, one radiologist (Zhujiang Hospital of Southern Medical University, China) reviewed and confirmed all ROIs to ensure the quality and consistency of tumor delineation.

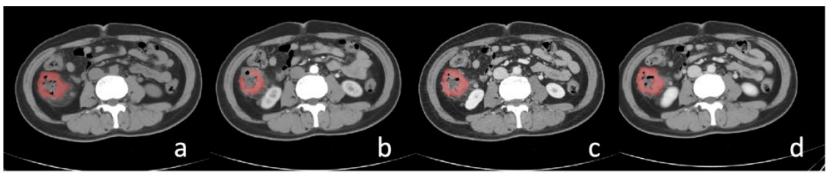

Figure 1. The figure illustrated the delineated ROIs of a 65-year-old female patient diagnosed with right colon cancer across four phases. The colon cancer lesions were depicted in the non-enhanced phase (a), arterial phase (b), portal venous phase (c), and delayed phase (d) CT axial images; Abbreviation: ROI, region of interest

Histopathology

The histopathological diagnosis followed the guidelines outlined in the 8th edition of the American Joint Committee on Cancer staging standard (11). As per this classification, T1–T2 stages were designated as early stages, whereas T3–T4 stages were categorized as locally advanced stages.

Feature Extraction

Before feature computation, standardization of CT image pixel sizes was performed across the four phases through resampling, achieving a consistent size of $1 \times 1 \times 3\ mm$. Subsequently, leveraging PyRadiomics (version 3.0, Python 3.10, accessible at https://pyradiomics.readthedocs.io/en/latest/), a total of 4,872 quantitative imaging features were extracted from these standardized CT images. Specifically, each phase—non-enhanced, arterial, portal venous, and delayed—yielded 1,218 distinct features.

The extracted features were categorized into three main groups: (1) First-order statistics: comprising 18 descriptors, this category quantifies voxel intensity distribution within the CT images using fundamental statistical metrics. (2) Shape-based features: encompassing 14 3D features, this group characterizes the shape and size attributes of the segmented regions. (3) Texture features: derived from calculations involving the gray level co-occurrence matrix (GLCM, 22 features), gray level run length matrix (GLRLM, 16 features), gray level size zone matrix (GLSZM, 16 features), and gray level dependence matrix (GLDM, 14 features), this group included 68 features that quantified heterogeneity variations within the region of interest.

Moreover, based on the first-order statistics and texture features, an additional 430 features were derived using Laplacian of Gaussian (Log) transformation, while 688 features were obtained through wavelet transform.

Feature Selection

Before the feature selection process, normalization was conducted to achieve uniform scaling of radiomic features. Recognizing the computational burden imposed by high-dimensional features and the potential compromise in classification accuracy due to redundant features, steps were taken to mitigate these concerns. Z-score normalization was employed to standardize the radiomic features, ensuring their range fell within the range of 0-1. This normalization process was intended to enhance the identification of the most pertinent features crucial for effective T-staging (T1-T2 vs. T3-T4) classification tasks.

After normalization, two distinct feature selection techniques were applied. First, the minimum redundancy maximum relevance (mRMR) method was employed to extract the top 20 features with the highest mRMR scores, identified as significant contributors. Subsequently, the LASSO logistic regression method underwent a 10-fold cross-validation process on the training dataset, consisting of 135 cases. This step determined the tuning parameter λ (12) and identified the optimal number of features with a more substantial influence on T staging.

Model Building

A LASSO logistic regression model was constructed, enhancing its performance via penalty parameter tuning within a 10-fold cross-validation framework. A radiomic score (Rad-score) was computed for each patient, signifying the significance of individual features based on their respective LASSO coefficients. Further metrics, including receiver operating characteristic curves (ROC) curves, area under the ROC curve (AUC) values, accuracy, sensitivity, and specificity, were computed accordingly. Finally, a comparison of the AUC estimates derived from predictive models was conducted using the Delong non-parametric method.

Results and Discussion

Study Population

The study enrolled a cohort of 191 patients, with an average age of 61.87 ± 13.137 years. Females constituted 43.5% of the total cohort. When stratified by the T-staging system, 75 cases were categorized as T1-T2 staging, including 47 males and 28 females, with a mean age of 61.267 ± 11.02 years. Meanwhile, 116 cases fell into the T3-T4 staging category, comprising 61 males and 55 females, with a mean age of 62.26 ± 14.37 years.

The training set comprised 135 cases, consisting of 53 early-stage (T1-T2) and 82 advanced-stage (T3-T4) patients. Conversely, the test set encompassed 56 cases, with 22 early-stage and 34 advanced-stage patients. Table 1 presents an overview of baseline clinical data and patient cohort.

Table 1. The basic information of patients

	Early Staging (75)	Advanced staging (116)
Age (average±SD)	61.267 ±11.02	62.26±14.37
Female	28	55
Male	47	61
T staging		
T1	26	/
T2	49	/
T3	/	79
T4	/	37
Training data	53	82
Testing data	22	34

Feature Extraction

After employing the mRMR feature selection method, the top 20 features with the highest mRMR scores were selected from each phase. Subsequently, LASSO logistic regression with 10-fold cross-validation was performed. The resulting binomial deviances and coefficients, tuned with different factors (λ), were visualized in Figure 2 A1, B1, C1, and D1. Ultimately, a set of 34 non-zero coefficient features was chosen: 7 for the non-enhanced phase, 11 for the arterial phase, 6 for the portal venous phase, and 10 for the delayed phase, as depicted in Figure 2 A3, B3, C3, and D3 (refer to Table 2). These features were associated with corresponding optimal λ values of 0.024, 0.015, 0.039, and 0.026, respectively, elucidated in Figure 2 A1, B1, C1, and D1.

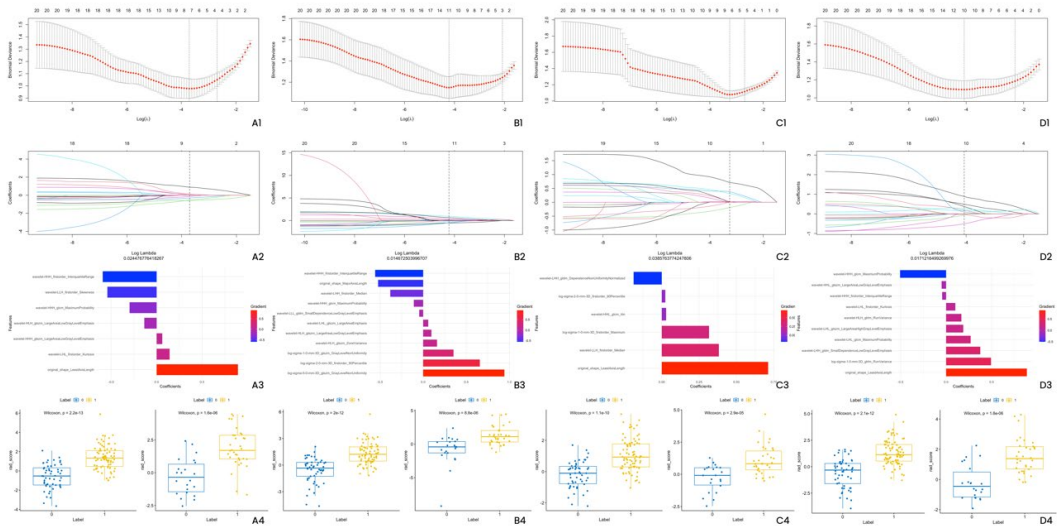

Figure 2. illustrates the key steps in the model selection process using ten-fold cross-validation to identify the optimal parameter (λ), denoted by the minimal criterion and the 1-standard error (SE) of the minimum criterion marked by vertical lines in A1, B1, C1, and D1. A2, B2, C2, and D2 depicted the Least Absolute Shrinkage and Selection Operator (LASSO) coefficient profiles showcasing the features with nonzero coefficients. The selected features' corresponding coefficients were presented in A3, B3, C3, D3. Lastly, A4, B4, C4, and D4 demonstrated the radiomics signature (Rad Score)

These selected features encompassed shape and wavelet features in the non-enhanced phase, while the arterial, portal venous, and delayed phases exhibited LoG, wavelet, and shape features. Notably, the 'original_shape_LeastAxisLength' feature consistently exhibited the highest coefficient across the non-enhanced, arterial, portal venous, and delayed phases. Additionally, all phases incorporated wavelet features (Table 2, Figure 2 A3, B3, C3, D3).

Table 2. The non-zero coefficient features were chosen in each of the four phases

Phase	Feature	coefficients
Non-enhance phase	original_shape_LeastAxisLength	0.894
	wavelet-LHL_firstorder_Kurtosis	0.142
	wavelet-HHH_glszm_LargeAreaLowGrayLevelEmphasis	0.062
	wavelet-HLH_glszm_LargeAreaLowGrayLevelEmphasis	-0.136
	wavelet-HHH_glcm_MaximumProbability	-0.298
	wavelet-LLH_firstorder_Skewness	-0.542
	wavelet-HHH_firstorder_InterquartileRange	-0.593
Arterial phase	log-sigma-5-0-mm-3D_glszm_GrayLevelNonUniformity	0.942
	log-sigma-2-0-mm-3D_firstorder_90Percentile	0.657
	log-sigma-1-0-mm-3D_glszm_GrayLevelNonUniformity	0.352
	wavelet-HLH_glszm_ZoneVariance	0.160
	wavelet-HLH_glszm_LargeAreaLowGrayLevelEmphasis	0.096
	wavelet-LHL_glszm_LargeAreaEmphasis	0.058
	wavelet-LLL_gldm_SmallDependenceLowGrayLevelEmphasis	-0.046
	wavelet-HHH_glcm_MaximumProbability	-0.109
	wavelet-LHH_firstorder_Median	-0.382
	original_shape_MajorAxisLength	-0.523
	wavelet-HHH_firstorder_InterquartileRange	-0.557
Portal venous phase	original_shape_LeastAxisLength	0.712
	wavelet-LLH_firstorder_Median	0.382
	log-sigma-1-0-mm-3D_firstorder_Maximum	0.316
	wavelet-HHL_glcm_Idn	0.029
	log-sigma-2-0-mm-3D_firstorder_90Percentile	0.024
	wavelet-LHH_gldm_DependenceNonUniformityNormalized	-0.188
Delayed phase	original_shape_LeastAxisLength	0.887
	log-sigma-1-0-mm-3D_glrlm_RunVariance	0.493
	wavelet-LHH_gldm_SmallDependenceLowGrayLevelEmphasis	0.375
	wavelet-LHL_glcm_MaximumProbability	0.269
	wavelet-LHL_glszm_LargeAreaHighGrayLevelEmphasis	0.188
	wavelet-HLH_glrlm_RunVariance	0.167
	wavelet-LHL_firstorder_Kurtosis	0.101
	wavelet-HHH_firstorder_InterquartileRange	-0.044
	wavelet-HHL_glszm_LargeAreaLowGrayLevelEmphasis	-0.049
	wavelet-HHH_glcm_MaximumProbability	-0.507

Model Performance

In both the training and test sets across all four phases, the radiomics signature (Rad Score) for T3-T4 stage patients surpassed that of T1-T2 stage patients (all $P < 0.001$). This signature was derived from the selected features and their corresponding coefficients, as depicted in Figure 2 A4, B4, C4, and D4.

In the training set, the AUC values for the non-enhanced, arterial, portal venous, and delayed phases were 0.87 (95% CI 0.82-0.93), 0.86 (95% CI 0.80-0.92), 0.83 (95% CI 0.76-0.90), and 0.86 (95% CI 0.80-0.92), respectively. Corresponding accuracy values were 0.77, 0.81, 0.76, and 0.78, sensitivities were 0.91, 0.79, 0.74, and 0.87, and specificities were 0.68, 0.82, 0.78, and 0.72 (Table 3, Figure 3 A1, B1, C1, D1). The DeLong test indicated no statistically significant differences in the AUC values among the four phases in the training set ($P = 0.3233$-0.7213, Table 4).

Table 3. The evaluations of performance in each of the four phases

Phase	dataset	AUC	P value	Accuracy	Sensitivity	Specificity
Non-enhance phase	Train	0.87(0.82-0.93)	0.7896	0.77	0.91	0.68
	Test	0.86(0.76-0.96)		0.84	0.73	0.91
Arterial Phase	Train	0.86(0.80-0.92)	0.7221	0.81	0.79	0.82
	Test	0.84(0.73-0.94)		0.80	0.64	0.91
Portal venous phase	Train	0.83(0.76-0.90)	0.8739	0.76	0.74	0.78
	Test	0.82(0.71-0.93)		0.75	0.86	0.68
Delayed phase	Train	0.86(0.80-0.92)	1	0.78	0.87	0.72
	Test	0.86(0.75-0.97)		0.88	0.68	1.00

In the test set, the AUC values for the non-enhanced, arterial, portal venous, and delayed phases were 0.86 (0.76-0.96), 0.84 (0.73-0.94), 0.82 (0.71-0.93), and 0.86 (0.75-0.97), respectively. The accuracy values were 0.84, 0.80, 0.75, and 0.88, sensitivities were 0.73, 0.64, 0.86, and 0.68, and specificities were 0.91, 0.91, 0.68, and 1.00 (Table 3, Figure 3 A2, B2, C2, D2). The DeLong test revealed no statistically significant differences in the AUC values among the four phases in the test set (P = 0.5413-0.9912, Table 4).

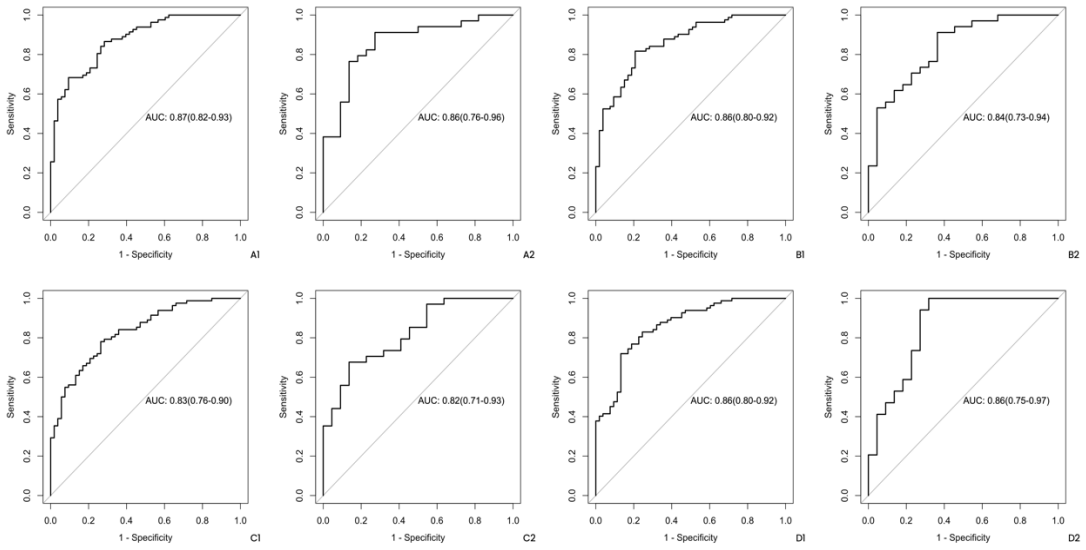

Figure 3. The ROC curves among each of the four phases are displayed for both the train and test sets. In the train set, the labels representing the non-enhanced, arterial, portal venous, and delayed phases were A1, B1, C1, and D1, respectively. In the test set, the labels corresponding to the non-enhanced, arterial, portal venous, and delayed phases were A2, B2, C2, and D2, respectively

No statistically significant differences were observed in the AUC values between the training and test sets in each of the four phases (P = 0.7221-1). Overall, each phase demonstrated good predictive performance in both the training and test sets, with the highest AUC value reaching 0.86 and the highest precision reaching 0.88 in the test set.

Table 4. The P values across four phases in both train and test sets

Train	N ROC	A ROC	P ROC
A ROC	0.7213	/	/
P ROC	0.3233	0.5302	/
D ROC	0.7151	0.9919	0.5389
Test			
A ROC	0.7629	/	/
P ROC	0.5988	0.8242	/
D ROC	0.9912	0.7284	0.5413

Abbreviations: N, non-enhanced phase; A, arterial phase; P, Portal venous phase; D, Delayed phase; ROC, receiver operating characteristic curves.

Discussion

Early and accurate diagnosis, along with precise clinical staging of colon cancer, significantly influences the prognosis and guides treatment strategies. In this study, leveraging multi-phase CT scans and employing radiomics methods, we aimed to distinguish between T1-T2 and T3-T4 stages across each phase. Our results indicated that radiomics showcased remarkable predictive performance using multi-phase CT images in both the training and test datasets.

Accurate preoperative staging not only helps avoid unnecessary overtreatment but also contributes to improved postoperative survival rates among colon cancer patients. CT imaging has conventionally been an integral component of colon cancer evaluations, primarily to rule out distant disease. While CT provides precise information regarding tumor size and potential invasion into surrounding organs and structures, its accuracy in differentiating between various T stages (T1-T4) is limited due to insufficient soft tissue contrast resolution. These limitations are supported by a meta-analysis (13), suggesting that CT's accuracy in colon cancer staging falls short of ideal standards. Consequently, there is a pressing need for alternative risk stratification methods using CT imaging. Radiomics has emerged as a prominent field within radiology in recent years. Several applications have demonstrated the potential of utilizing routinely acquired radiographic data to predict genetic phenotypes, prognosis, and potential responses to treatment (14-16).

Multivariable logistic regression has become widely utilized in recent research studies, ranging from predicting muscle invasion status in bladder cancer (17) to forecasting the enlargement of intracerebral hemorrhage (18) and preoperative classification of ovarian cysts (19). In this study, we developed and validated a multi-phase CT radiomics model to distinguish between T1-T2 and T3-T4 staging in colon cancer patients. By extracting features from non-enhanced, arterial, portal venous, and delayed phases, we covered the entire tumor and identified independent predictive factors for distinguishing between T1-T2 and T3-T4 staging using LASSO logistic regression. Our investigation involved employing LASSO logistic regression to validate the T staging (T1-T2 versus T3-T4) performance across different phases. In the test set, AUC values ranged from 0.82 to 0.86 for the four phases, with the non-enhanced and delayed phases exhibiting the highest performance at 0.86. The accuracy across the four phases varied from 0.75 to 0.88, with the delayed phase achieving the highest accuracy at 0.88 (see Table 3). DeLong's test results revealed no significant differences in the AUC values between the four phases in the test set (P = 0.5413-0.9912). Similarly, there were no significant differences observed in the AUC values between the four phases in both the training and test sets (P = 0.7221-1). Additionally, we conducted a comparative analysis of staging performance (T1-T2 vs T3-T4) utilizing portal vein images in conjunction with the expertise of radiologists (XX). Our findings revealed that within the test set, the radiomic AUC values for staging surpassed those derived from the radiologists' expertise (AUC = 0.72, 95% CI (0.61-0.72)).

Overall, all phases demonstrated good predictive performance in both the test and training sets, with the highest AUC value reaching 0.86 and the highest accuracy at 0.88. Hong *et al*. (8) conducted a logistic regression analysis of portal venous CT images in primary surgically resected colon cancer patients to ascertain the relationship between radiomic features and high-risk (T3-T4) colon tumors. They established a combined model of radiomics and CT staging, achieving an AUC of 0.799 (95% CI: 0.720-0.839). In our study, the AUC for the portal venous phase in the training set was 0.83 (95% CI: 0.76-0.90), and the sensitivity and specificity were 0.74 and 0.78, respectively. For the portal venous phase

in the test set, the AUC was 0.82 (95% CI: 0.71-0.93), and the sensitivity and specificity were 0.76 and 0.74, respectively.

Given the limited research on CT radiomics in distinguishing colon cancer staging between T1-T2 and T3-T4 stages, we compared our findings with some MR radiomics-related research in rectal cancer patients between T1-T2 and T3-T4 stages. Our diagnostic performance exceeded theirs. For instance, Liu *et al*. (20) performed a texture feature analysis of ADC maps from MRI images of 68 rectal cancer patients, providing valuable information for identifying locally advanced rectal cancer, with an AUC of 0.743. Additionally, Dou *et al*. (21) utilized LASSO regression to predict essential factors for high-risk rectal staging (T3-T4 staging) in rectal cancer patients, achieving an AUC of 0.85. Meanwhile, Ma *et al*. (10) used MRI radiomics extracted from T2-weighted images to predict pathological features of rectal cancer, employing the LASSO method for optimal feature selection. Their findings revealed 11 features associated with T (T1-T2 and T3-T3) staging, achieving a prediction accuracy of 0.762.

In our study, we conducted feature extraction from both original images and images processed through various filters, such as wavelet and LoG filters. The major proportion of features utilized to construct the Rad Score predominantly originated from images filtered through the wavelet technique (outlined in Table 2). Wavelet filtering, known for its effectiveness in signal denoising, has gained substantial traction and application in recent research endeavors (22, 23). For instance, a prospective investigation that predicted radiomic features for grading rectal cancer tumors primarily relied on features derived from wavelet-filtered images (22). This aligns with Ma *et al*.'s findings (10), where weighted MRI images were employed to extract radiomic features for predicting pathological characteristics in rectal cancer.

Moreover, in the prediction of pathological responses (23) and liver metastasis in rectal cancer patients (24), the predominant features were extracted from wavelet-filtered images. Furthermore, the inclusion of the "original_shape_LeastAxisLength" feature across non-enhanced, portal venous, and delayed phases, demonstrating the highest coefficient, emphasized the crucial role of the shortest axis shape feature in staging colon cancer. This finding aligns with results from some studies (25, 26) indicating the discriminative capability of tumor size in staging.

Despite these significant findings, our study faces certain limitations. Firstly, our sample size is relatively restricted, and the absence of external validation limits the ability to confirm the model's performance. In future research, we intend to continue this study by incorporating data from other hospitals and establishing a multi-center study to validate our model further. Secondly, all images were obtained from CT scanners produced by a single manufacturer, which may limit the generalizability of the model and could affect the accuracy of staging predictions when using CT scanners from other manufacturers. To address this, we plan to include colon cancer data from CT scanners of different manufacturers in future studies to further refine our staging model. Thirdly, our study did not incorporate clinical laboratory indicators or integrate them with radiomic scores for combined predictive analysis. In future studies, we aim to collect data from patients with comprehensive clinical information to develop a combined model that integrates clinical and radiomic features, thereby enhancing the model's predictive power. Finally, due to data confidentiality, we were unable to obtain data from previously published studies for validation purposes, which constitutes one of the limitations of this study.

Conclusions

In conclusion, our findings demonstrated that multi-phase CT radiomics exhibited high performance in distinguishing between early (T1 -T2) stage and advanced (T3 -T4) stage colon cancer, with the highest AUC reaching 0.86. These results held significant value for accurately staging patients with colon cancer and guiding neoadjuvant treatments.

Conflicts of Interest

The authors of this manuscript declare no relationships with any companies whose products or services may be related to the subject matter of the article.

Ethical Statement

The authors are accountable for all aspects of the work in ensuring that questions related to the accuracy or integrity of any part of the work are appropriately investigated and resolved. The study was conducted

following the Declaration of Helsinki (as revised in 2013). The study was approved by the institutional ethics board of Zhujiang Hospital of Southern Medical University and individual consent for this retrospective analysis was waived.

Acknowledgement

This work is part of a research project, FS202402006, supported by The Scientific Research Funding Project of the Nanfang Medical Imaging Alliance. At the same time, the authors express their deep gratitude for the outstanding support and research-friendly environment offered by Universiti Teknologi Malaysia (UTM). The research received funding from UTM Fundamental Research (UTMFR) under cost centre number Q.J130000.3823.23H68

References

[1] Abdullah Thaidi, N. I., Mat Jusoh, H., Ghazali, A. B., Susanti, D., & Haron, N. (2019). The effect of bioactive polyphenols from *Anacardium occidentale* Linn. leaves on alpha-amylase and dipeptidyl peptidase IV activities. *Indonesian Journal of Chemistry*.

[2] Abdullahi, S., & Olatunji, G. A. (2010). Antidiabetic activity of *Anacardium occidentale* in alloxan–diabetic rats. *Journal of Science and Technology, 30*(3), 35–39.

[3] Agius, L. (2008). Targeting hepatic glucokinase in type 2 diabetes: Weighing the benefits and risks. *Diabetes, 58*(1), 18–20.

[4] Aracelli, de S. L., Md., T. I., Antonio, L. G. J., Joao, M. de C. e S., Marcus, V. O. B. de A., Marcia, F. C. J. P., *Jose, A. D. L.* (2016). Pharmacological properties of cashew (*Anacardium occidentale*). *African Journal of Biotechnology, 15*(35), 1855–1863.

[5] Baig, M. H., Ahmad, K., Rabbani, G., Danishuddin, M., & Choi, I. (2018). Computer aided drug design and its application to the development of potential drugs for neurodegenerative disorders. *Current Neuropharmacology, 16*(6), 740–748.

[6] Baptista, A., Gonçalves, R. V., Bressan, J., & do Carmo Gouveia Pelúzio, M. (2018). Antioxidant and antimicrobial activities of crude extracts and fractions of cashew (*Anacardium occidentale* L.), caju (*Anacardium microcarpum*), and pequi (*Caryocar brasiliense* C.): A systematic review. *Oxidative Medicine and Cellular Longevity*.

[7] Berg, J. M., Tymoczko, J. L., & Stryer, L. (2002). *Biochemistry: Section 1.3, Chemical bonds in biochemistry* (5th ed.). New York, NY: W H Freeman.

[8] Chotphruethipong, L., Benjakul, S., & Kijroongrojana, K. (2019). Ultrasound assisted extraction of antioxidative phenolics from cashew (*Anacardium occidentale* L.) leaves. *Journal of Food Science and Technology*.

[9] Dias, C. C. Q., Madruga, M. S., Pintado, M. M. E., Almeida, G. H. O., Alves, A. P. V., Dantas, F. A., … *Soares, J. K. B.* (2019). Cashew nuts (*Anacardium occidentale* L.) decrease visceral fat, yet augment glucose in dyslipidemic rats. *PLOS ONE, 14*(12).

[10] El-Kabbani, O., Ruiz, F., Darmanin, C., & Chung, R. P.-T. (2004). Aldose reductase structures: Implications for mechanism and inhibition. *Cellular and Molecular Life Sciences (CMLS), 61*(7-8), 750–762.

[11] Fikrika, H., Ambarsari, L., & Sumaryada, T. (2016). Molecular docking studies of catechin and its derivatives as anti-bacterial inhibitor for glucosamine-6-phosphate synthase. *IOP Conference Series: Earth and Environmental Science, 31*, 012009.

[12] Hebert, L. F., Jr, Daniels, M. C., Zhou, J., Crook, E. D., Turner, R. L., Simmons, S. T., Neidigh, J. L., Zhu, J. S., Baron, A. D., & McClain, D. A. (1996). Overexpression of glutamine amidotransferase in transgenic mice leads to insulin resistance. *The Journal of Clinical Investigation, 98*(4), 930–936.

[13] Hubbard, R. E. (2010). Hydrogen bonds in proteins: Role and strength. *February*.

[14] Hyun, T. K., Eom, S. H., & Kim, J. (2014). Molecular docking studies for discovery of plant-derived α-glucosidase inhibitors. *7*(3), 166–170.

[15] Kalhotra, P., Chittepu, V. C., Osorio-Revilla, G., & Gallardo-Velázquez, T. (2019). Discovery of galangin as a potential DPP-4 inhibitor that improves insulin-stimulated skeletal muscle glucose uptake: A combinational therapy for diabetes. *International Journal of Molecular Sciences, 20*(5), 1228.

[16] Klvana, M. (2018). Re: The number and distance of H-bond formed between protein-ligand complex varies in 2 different softwares, how it is possible?

[17] Kondo, H., Fujimoto, K. J., Tanaka, S., Deki, H., & Nakamura, T. (2015). Theoretical prediction and experimental verification on enantioselectivity of haloacid dehalogenase L-DEX YL with chloropropionate. *Chemical Physics Letters*.

[18] Mohammed, A., Kumar, D., & Rizvi, S. I. (2015). Antidiabetic potential of some less commonly used plants in traditional medicinal systems of India and Africa. *Journal of Intercultural Ethnopharmacology, 4*(1).

[19] Natarajan, A., Sugumar, S., Bitragunta, S., & Balasubramanyan, N. (2015). Molecular docking studies of (4Z, 12Z)-cyclopentadeca-4, 12-dienone from *Grewia hirsuta* with some targets related to type 2 diabetes. *BMC Complementary and Alternative Medicine, 15*(1).

[20] National Center for Biotechnology Information. PubChem Database. Phenol, CID=996.

[21] Nur Athirah Zabidi, N., Nur Akmal Ishak, M., Muhajir Hamid, S., Siti Efliza Ashari, & Muhammad Alif Mohammad Latif. (2021). Inhibitory evaluation of *Curculigo latifolia* on α-glucosidase, DPP (IV) and in vitro studies in antidiabetic with molecular docking relevance to type 2 diabetes mellitus. *Journal of Enzyme Inhibition and Medicinal Chemistry, 36*(1), 109–121.

[22] Nurul Iilani, A. H. (2015). Affinity of dehalogenase E towards various haloalkanoic acids. *International Islamic University Malaysia, Kuantan*.
[23] Okpashi, V. E., Bayim, P. R. B., & Obi-Abang, M. (2014). Comparative effects of some medicinal plants: *Anacardium occidentale, Eucalyptus globulus, Psidium guajava,* and *Xylopia aethiopica* extracts in alloxan-induced diabetic male Wistar albino rats. *Biochemistry Research International*.
[24] Rizvi, S. I., & Mishra, N. (2013). Traditional Indian medicines used for the management of diabetes mellitus. *Journal of Diabetes Research*.
[25] Ross, I. A. (2001). *Anacardium occidentale*. In *Medicinal plants of the world* (2nd ed., pp. 43–45). Humana Press.
[26] Salehi, G., Gültekin-Özgüven, K., Kırkın, Özçelik, Morais-Braga, Carneiro, Bezerra, *et al.* (2019). Anacardium plants: Chemical, nutritional composition and biotechnological applications. *Biomolecules, 9*(9), 465.
[27] Schulze-Kaysers, N., Feuereisen, M. M., & Schieber, A. (2015). Phenolic compounds in edible species of the Anacardiaceae family – a review. *RSC Advances, 5*(89), 73301–73314.
[28] Shen, W., & Lu, Y. H. (2013). Molecular docking of citrus flavonoids with some targets related to diabetes. *Bangladesh Journal of Pharmacology, 8*(2), 156–170.
[29] Thallapally, P. K., & Nangia, A. (2001). A Cambridge Structural Database analysis of the C–H … Cl interaction: C–H … Cl2 and C–H … Cl–M often behave as hydrogen bonds but C–H … Cl–C is generally a van der Waals interaction, 1–6.
[30] Wallace, A. C., Laskowski, R. A., & Thornton, J. M. (1995). LIGPLOT: A program to generate schematic diagrams of protein-ligand interactions. *Clean up structure, 8*(2), 127–134.
[31] World Health Organization. (2020). Diabetes. Retrieved from https://www.who.int/news-room/fact-sheets/detail/diabetes
[32] Yuan, H., Ma, Q., Ye, L., & Piao, G. (2016). The traditional medicine and modern medicine from natural products. *Molecules, 21*.